https://doi.org/10.17221/60/2023-SWR

Seasonal variations of vegetative indices and their correlation with evapotranspiration and soil water storage in a small agricultural catchment

Tailin Li[1], Massimiliano Schiavo[2], David Zumr[1]*

[1]*Department of Landscape Water Conservation, Faculty of Civil Engineering, Czech Technical University in Prague, Prague, Czech Republic*
[2]*Dipartimento di Ingegneria Civile e Ambientale, Politecnico di Milano, Milano, Italy*

**Corresponding author: tailin.li@fsv.cvut.cz*

Citation: Li T.L., Schiavo M., Zumr D. (2023): Seasonal variations of vegetative indices and their correlation with evapotranspiration and soil water storage in a small agricultural catchment. Soil & Water Res., 18: 246–268.

Abstract: A precise measurement of evapotranspiration (ET) and soil water storage (SWS) is necessary for crop management and understanding hydrological processes in agricultural catchments. In this study, we extracted the vegetative indices (VIs, including normalised difference vegetation index (NDVI), soil-adjusted vegetation index (SAVI), and enhanced vegetation index (EVI)) from satellite images of the Nučice catchment. We found a consistent seasonal pattern of VIs across the catchment with higher values and variation ranges during spring and summer and lower values and variation ranges during autumn and winter. Spatial variation of VIs also followed a seasonal trend, decreasing during crop growth and increasing after crop harvesting. Seasonal correlations were observed between monthly average ET and SWS with VIs throughout one crop season, which can be expressed mathematically as exponential functions. We propose that VIs can be used as a surrogate measure for ET and SWS in catchments with poor monitoring capabilities. Further studies are required to investigate the spatial distribution of ET and SWS throughout the watershed and their relationship with VIs. Furthermore, our research emphasises the importance of subsurface recharge in the water balance of the investigated fields. It suggests that subsurface flow may be influenced by potential gradients of the water table, driving its seasonal behaviour in response to bedrock morphology.

Keywords: catchment hydrology; remote sensing; soil moisture; water balance

When it comes to crop management and understanding hydrological processes in agricultural catchments, an accurate estimation of evapotranspiration (ET) and soil moisture is essential (Zhang & Wegehenkel 2006; Park et al. 2017; Cheng et al. 2022a). Evapotranspiration represents the combined loss of water from the soil through evaporation and from the plant canopy through transpiration, while soil moisture is an essential indicator of soil health and water availability for crops. However, ET and soil moisture are two of the most challenging elements of the water cycle to monitor on field to regional scales because of the uncertainty introduced by land surface heterogeneity and environmental restrictions (Wang et al. 2006; Martínez & Gilabert 2009; Allen et al. 2011b; He et al. 2019; Wyatt et al. 2021). Fur-

Supported by the Czech Technical University in Prague's Grant Agency, under Grant No. SGS23/155/OHK1/3T/11, and the LTAUSA19019 project "Connectivity of sediment transport within intensively-used rural catchments" supported by the Ministry of Education, Youth and Sports of the Czech Republic, and TUdi Project, EU Horizon 2020 Grant Agreement No. 101000224.

https://doi.org/10.17221/60/2023-SWR

thermore, catchments with high levels of agricultural activity pose supplementary obstacles, as agricultural practices and land management often hinder effective monitoring of evapotranspiration and soil moisture (Hébrard et al. 2006; Rong et al. 2017).

Various methods have been developed for measuring ET and soil moisture. Traditional methods for measuring ET include the soil water balance method, lysimeters, the Bowen Ratio Energy Balance (BREB), Eddy covariance (EC), scintillometers, and sap flow methods (Allen et al. 2011a). The soil water balance method (Jensen & Wright 1978; Cholpankulov et al. 2008) estimates ET by simply measuring soil moisture changes over time. Similarly, lysimeters (Howell et al. 1995; Marek et al. 2006) allow for direct measurement of ET by collecting and measuring the water that is lost through evapotranspiration. On the other hand, the BREB method (Bowen 1926; Angus & Watts 1984; Devitt et al. 1998) involves measuring energy exchange at the surface to estimate ET. Likewise, the EC method (Wilson et al. 2002; Baldocchi 2003) measures heat and gas exchange in the atmospheric boundary layer above the vegetation and calculates the vertical water vapour fluxes. Scintillometers are optical sensors that measure turbulence by analysing the scattering and fluctuation of light as it passes through the atmosphere, providing estimations of heat fluxes that can be linked to ET (Meijninger et al. 2002). The sap flow approach, on the other hand, directly monitors the water flow within plant stems or trunks, thus quantifying plant transpiration, which is a component of ET (Granier 1987).

Soil moisture is another critical variable in the water cycle, referring to the amount of water stored in the soil profile. Common approaches to assessing soil moisture include direct soil sampling, and in-situ measurements using time-domain reflectometry (TDR) or time-domain transmissometry (TDT) sensors. Direct soil sampling (Famiglietti et al. 1998) involves physically removing soil from a given location and weighing it before and after drying to determine moisture content. In-situ methods (Robinson et al. 2003; Bogena et al. 2010) such as TDR or TDT sensors use probes inserted into the soil to measure the electrical permittivity (Topp et al. 1980) of the soil, which is then used to estimate soil moisture content.

However, these on-site measurements are usually constrained by spatial and temporal resolution and the expense of a dense sensor network (He et al. 2019). In recent years, researchers have increasingly turned to satellite imagery to understand ET and soil moisture at large scales (from the regional to the global level). Satellite-derived vegetation indices (VIs) are commonly used in agricultural fields to monitor the dynamics of plant growth and to estimate important biophysical parameters, such as leaf area index, biomass, and chlorophyll content (Tucker 1979; Gitelson et al. 1996). Further, VIs such as the normalised difference vegetation index (NDVI) (Rouse et al. 1973), the soil-adjusted vegetation index (SAVI) (Huete 1988), and the enhanced vegetation index (EVI) (Gao 2000; Huete et al. 2002) can also be used to predict ET and root-zone soil moisture. By combining the NDVI, SAVI, and surface temperature obtained from satellite images, and with the evapotranspiration Priestley-Taylor model (Priestley & Taylor 1972), Fisher et al. (2008) were able to create monthly maps at the global scale of ET and verify them using local observations. Alternatively, many studies (Zhang & Wegehenkel 2006; Yuan et al. 2010; Park et al. 2017) exploited satellite-derived vegetation indices to determine the crop coefficient (Kc) and then multiplied the Kc by the reference evapotranspiration (calculated based on FAO-56 (Allen et al. 1998)) to estimate the actual ET. Moreover, VIs retrieved from optical remote sensing datasets can also be utilised in assessing soil moisture observation. For example, with a combination of NDVI snapshots and in-situ meteorological data, some studies (Crow et al. 2008; Wyatt et al. 2021) estimated the soil moisture dynamics in root zone under various land cover types using a simple water balance model based on the FAO-56 dual crop coefficient approach (Allen et al. 1998). To further enhance the soil moisture estimate, several studies used the remote sensing-based datasets with the physically based model (Zhang & Wegehenkel 2006; Benninga et al. 2022), random forest regression (Cheng et al. 2022b) and machine learning method (Abowarda et al. 2021; Cheng et al. 2022a; Nguyen et al. 2022).

Because of the limitations given by the occasional occurrence of cloud cover and generally low spatial-temporal resolution, satellite imagery is widely used for large-scale studies; nevertheless, small-scale spatial variations in evapotranspiration and soil water storage patterns must also be considered. Since in the small catchments, both farmers and water management can benefit from a better understanding of the spatial and temporal fluctuations in evapotranspiration and soil water storage within individual fields, as this knowledge drives advances in precision agriculture and optimises harvest yields. To fill this information gap, many commercial companies, most notably Planet (http://www.planet.com), are pioneering the launch

https://doi.org/10.17221/60/2023-SWR

of CubeSats to offer high-resolution imagery (McCabe et al. 2017). Since then, several studies (Aragon et al. 2018, 2021; Houborg & McCabe 2018; Kimm et al. 2020; Ziliani et al. 2022) have been able to use cloud-free daily imagery of 3 m spatial resolution provided by CubeSats (from Planet) to enhance agricultural management on small field scales.

For historical reasons, most of the farmland in the Czech Republic consists of big, uniformly cultivated fields that are spread out over the country (Noreika et al. 2021). Despite their seemingly uniform appearance, the water balance within these fields may be influenced by various factors, including lateral subsurface flows (Tenreiro et al. 2022), topography and soil texture (Biswas 2019), or tillage direction (Jeřábek et al. 2022), which can alter the routing mechanism of water and sediment then further results in non-uniform distribution of soil water across the fields. Furthermore, even on a small-scale agricultural field, the surface energy balance may exhibit considerable variability due to the heterogeneity of land surface characteristics, vegetation cover, and microclimate conditions (Wohlfahrt & Tasser 2015). The spatiotemporal variation in the water and surface energy balance at a small-scale field could contribute to vegetation heterogeneity and manifest in the VIs obtained from satellite imagery. In the small-scale farmlands, however, the dynamics of satellite-derived VIs and their link with variations in ET and soil moisture remain largely unexplored. Hence, in this study, we have investigated cloud-free, high spatial and temporal resolution satellite images at the experimental catchment (Nučice) to understand: (*i*) how satellite-derived VIs are distributed across a uniform land use pattern? (*ii*) the temporal correlation between satellite-derived VIs and in-situ measurements of ET and soil moisture; (*iii*) the seasonal dynamics of the satellite-derived VIs and in-situ measurements of ET and soil moisture.

MATERIAL AND METHODS

Site description

The investigation was done in the experimental catchment of Nučice, Czech Republic. The watershed (0.531 km^2) has a mean elevation of 401 m a.s.l. (range from 382 to 417 m a.s.l.) with an average slope of 3.9% (ranging from 1% to 12%). The basin's outlet (49°57'49.230"N, 14°52'13.242"E) has been equipped with a gauging station since 2011. Since then, the catchment's hydrological and meteorological features have been observed. Based on the long-term regional measurements in the vicinity (Hanel et al. 2013), yearly precipitation averages 630 mm, the annual air temperature averages 6 °C, and annual evapotranspiration averages 500 mm, making the catchment's climate humid continental. The same land use pattern characterises the whole catchment area: more than 95% of the site is used for agricultural purposes, while the watercourse, riparian trees and bushes, and paved roads take up the remaining sections. The topsoil has a loamy texture with 13% clay, 42% silt, and 45% sand content. The watershed area is separated into three distinct agricultural fields (left, right, and top fields) (Figure 1). Due to the uni-

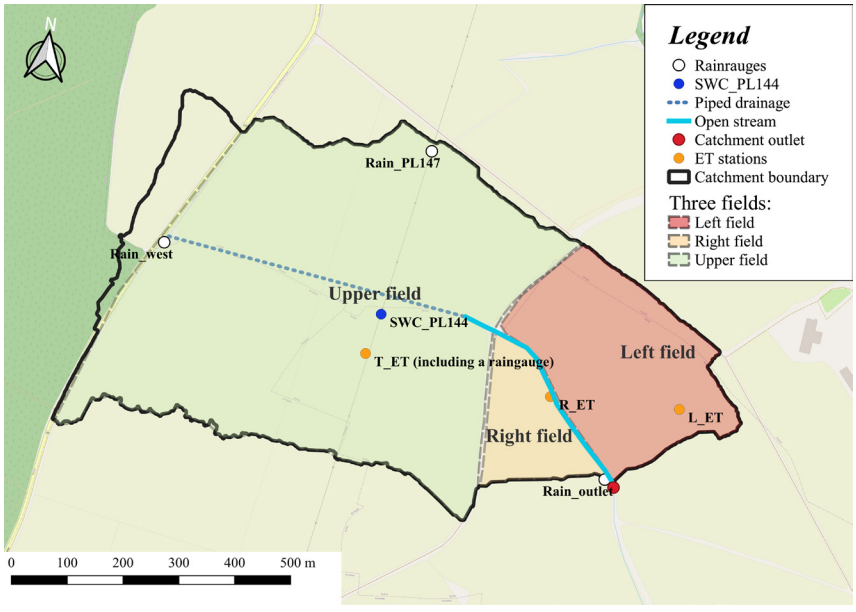

Figure 1. Meteorological and soil moisture measurements at the Nučice catchment

https://doi.org/10.17221/60/2023-SWR

form morphology and tillage practice in each field, the topsoil characteristics in each field are similar. (Zumr et al. 2015; Jeřábek et al. 2017; Li et al. 2021)

***In-situ* meteorological and soil water content (SWC) monitoring**

Since 2021, three meteorological stations (T_ET, L_ET, E_ET) have been deployed across three fields to measure evapotranspiration, each equipped with a net radiation sensor (NR Lite2, Kipp and Zonen, Netherlands) and all the sensors needed for the BREB calculation. In addition, one station (T_ET) has a four-component radiometer SN-500 (Apogee Instruments, USA). Data are captured and saved in data loggers every 10 min. The ET (mm/day) at each three ET stations were calculated based on the BREB equation (Bowen 1926; Irmak et al. 2014).

$$\lambda E = \frac{R_n - G}{1 + \beta} \quad (1)$$

where:

λE – the latent heat;

λ – the heat of water vaporisation;

E – the evapotranspiration;

R_n – the net radiation;

G – the soil heat flux density

β – the Bowen ratio, which can be expressed and calculated by the following equation:

$$\beta = \frac{H}{\lambda E} = \gamma \frac{\Delta T}{\Delta e} \quad (2)$$

where:

H – the sensible heat flux;

ΔT, Δe – the temperature and vapour pressure difference between the two measurement levels;

γ – the psychrometric constant.

Precipitation has been measured at four points (Rain_outlet, Rain_west, Rain_PL147, T_ET) throughout the catchment at intervals of 5 to 10 min. In this study, the average precipitation intensity calculated by averaging the data from the four stations was utilised.

Since the winter of 2019, CR650 soil water content reflectometers (Campbell Sci., UK) have been installed at depths of 10, 20, 30, 40, 50, and 60 cm for long-term measurement of soil water content in the centre of the catchment (SWC_PL144 in Figure 1). Prior to installation, all soil probes were calibrated, and they recorded data at hourly intervals. Soil water storage (SWS) was calculated by integrating the soil water content measurements across the entire profile (0–60 cm).

Satellite-based vegetation indices

We obtained cloud-free, high temporal (daily to weekly) images of high spatial resolution (3 m) from the PlanetScope imagery database, which is a constellation of 130 + CubeSats (4-kg satellites) (McCabe et al. 2017) maintained by the Planet company (http://www.planet.com). PlanetScope imagery is comprised of four spectral bands, including blue (455–515 nm), green (500–590 nm), red (590–670 nm), and near-infrared (NIR, 780–860 nm) (Cheng et al. 2020; Estes et al. 2022). Further, we retrieved the normalised difference vegetation index (NDVI) (Rouse et al. 1973), soil-adjusted vegetation index (SAVI) (Huete 1988) and enhanced vegetation index (EVI) (Gao 2000; Huete et al. 2002) based on the following equations:

$$\mathrm{NDVI} = \frac{\rho_{\mathrm{NIR}} - \rho_{\mathrm{red}}}{\rho_{\mathrm{NIR}} + \rho_{\mathrm{red}}} \quad (3)$$

$$\mathrm{SAVI} = 1.5 \times \frac{(\rho_{\mathrm{NIR}} - \rho_{\mathrm{red}})}{(\rho_{\mathrm{NIR}} + \rho_{\mathrm{red}} + 0.5)} \quad (4)$$

$$\mathrm{EVI} = \frac{2.5 \times (\rho_{\mathrm{NIR}} - \rho_{\mathrm{red}})}{(\rho_{\mathrm{NIR}} + 6 \times \rho_{\mathrm{red}} - 7.5 \times \rho_{\mathrm{blue}} + 1)} \quad (5)$$

where:

ρ_{NIR}, ρ_{red}, ρ_{blue} – the reflectance in the PlanetScope bands (near-infrared, red, and blue).

For data from January 2019 through September 2022, we calculated all of the VIs in the catchment (which covers most of the measuring time of the in-situ measurements). These calculations were performed using satellite pictures that were appropriately projected to maintain consistency in pixel structure. Further, to compare the VIs and local measurements, we retrieved the spatial mean VIs in each field and the buffer zone (20 m) surrounding each in-situ meteorological station and SWS nest. According to its size, each field has a different number of pixels (3 × 3 m): the top field has 41 099 pixels, the left field has 10 576 pixels, and the right field has 3 782 pixels. Moreover, each buffer zone contains 143 pixels.

Statistical analysis

Assessing variable associations through quantitative metrics. Cloud cover in the satellite images caused data gaps (mainly in spring and winter seasons)

https://doi.org/10.17221/60/2023-SWR

in our dataset, which reduced the data representation. The data were therefore averaged into a monthly time step. Further, each variable of interest (the monthly VIs, ET, and SWS) was collected within a seasonal ensemble during the measurement period. We used the coefficient of variance (*CV*) to quantify the spatial variability of the VIs across each field.

The correlation among all variables was modelled using simple linear or exponential functions (by using curve fitting function from Scipy Python library) to better understand the underlying trends and associations. Specifically, the following function was used to model the associations between monthly VIs and ET:

$$\mathrm{ET} = a \times e^{b \times \mathrm{VIs}} + c \tag{6}$$

whereas the relationships between monthly VIs and SWC or SWS were modelled using the exponential function shown below:

$$\mathrm{SWC\ or\ SWS} = a \times e^{-\left(\frac{X-b}{c}\right)^4} \tag{7}$$

where:

a, b, c – the fitting parameters for the optimisation.

Further, we evaluated the associations using the coefficient of determination () and root mean square error (RMSE):

$$r^2 = 1 - \frac{\mathrm{RSS}}{\mathrm{TSS}} \tag{8}$$

$$\mathrm{RMSE} = \sqrt{\frac{\sum_{i=1}^{n} (Y_{\mathrm{obs}} - Y_{sim})^2}{n}} \tag{9}$$

where:

RSS – the sum of squared residuals;

TSS – the total sum of squares;

Y_{obs}, Y_{sim} – the obaserved and simulated values (from fitted functions).

Seasonal analysis. To evaluate the seasonal variation, we based the seasonal dataset on monthly aggregated data to avoid null measurements, disregarding those when our instruments did not capture at least one of the measured quantities. At the monthly scale, the temporal sequence of the dataset was preserved for all the measured quantities. Furthermore, we normalised each monthly quantity upon its maximum value within the same month; hence all data were treated as real numbers within the unit interval. Finally, we aggregated the data at the seasonal scale through the usual convention employed in hydrological studies in Central Europe:

Spring = March, April, May (MAM)

Summer = June, July, August (JJA)

Autumn = September, October, November (SON)

Winter = December, January, February (DJF)

We aimed to evaluate the correlation quality between selected variables worthy of special attention in respect of the other ones. The selected ones are the measured ET in the three fields and the SWS from PL144 because it has a long and consistent measuring period and is in a representative location of the catchment.

We employed the Nash-Sutcliffe Efficiency Index (NSE; Nash & Sutcliffe 1970) to measure the temporal similarity between (*i*) ET and the other variables, and (*ii*) SWS and the other variables.

The NSE index is presented as follows:

$$\mathrm{NSE}_i = 1 - \frac{\sum_i \left(X_i - Y_i\right)^2}{\sum_i \left(X_i - \bar{X}_s\right)^2} \tag{10}$$

where:

i – the index referring to the i-th monthly entry, considered for a specific season s;

X_i – the i-th value of an independent variable;

X_s – its seasonal mean;

Y_i – the i-th dependent variable.

The NSE index ($-\infty$;1) is useful by informing about the biases between two variables, which must be temporarily homogeneous, and the sum of the variances of the independent variable. The closer to 1, the higher the similarity between two compared series of monthly variables aggregated at the seasonal scale.

Thus, we first evaluated NSE efficiency indices using ET for the left, right, and top fields (Figure 1) as independent variables and then considered SWS as the independent variable. Because of the high number of negative values of NSE to be considered, we preferred the Normalised Nash-Sutcliffe Efficiency index (NNSE, (0;1)) to the NSE version, with the former one written on a seasonal base as

$$\mathrm{NNSE}_i = \frac{1}{2 - \mathrm{NSE}_i} \tag{11}$$

The closer the seasonal NNSE index to 1, the higher the similarity between the ratio of the sums of monthly values of two variables X_i and Y_i, summed at the sea-

https://doi.org/10.17221/60/2023-SWR

sonal scale. NNSE values close to 1 mean that both the average bias between monthly-summed values and the variance of the independent variable is low, which lets us quantify how much to temporal series of two variables are mutually similar.

For each season, we evaluated the i-th NNSE, corresponding to the i-th month, and the range of variation of this similarity and its median value. To pursue this aim, we made use of seasonal boxplots, one for each field and seasonally divided, reporting the similarity between an independent variable (ET for left, right, and top field, then SWS) and another dependent one among those we monitored.

The similarity between the (empirical) probability distribution functions (PDF) of variables referring to different physical quantities might be challenging. Further steps toward a deeper statistical appraisal of considered quantities are needed to fully comprehend our data and how to relate different variables mutually. The path we followed to approach this issue is to recognise the first statistical moments of each (normalised) seasonal variable's PDF, to surrogate the behaviour of a PDF upon its statistical moments change across seasons. We first calculated four statistical moments at the seasonal scale for each variable we considered. The seasonal variables dataset we gather are firstly normalised, as well as we pointed out earlier in this Section. This way, seasonal statistical moments are between 0 and 1 for each considered season to ease their comparison. The seasonal moments we analyse are the mean, variance, skewness, and kurtosis for each normalised variable. These are enough to fully appraise variables' PDF (e.g. Schiavo et al. 2022) because they rule the density distribution of seasonally-aggregated data. The aim of doing such an analysis is that similarity in normalised statistical moments of the same order k, with $k = 1, 4$ here, enables us to assess whether two variables are statistically comparable. Moreover, the similarity (i.e. similar normalised statistical moments' values) of only one moment of a variable's distribution is not enough to sustain the former hypothesis; hence all the major statistical moments need to be calculated.

RESULTS AND DISCUSSION

The temporal and spatial variations of VIs. Spatial distribution and temporal patterns of vegetation indices in the following Figures. Figure 2 illustrates the monthly NDVI coverage of the study area (Figure 1) in 2022, which was later aggregated by season. Figure 3 and Figure 4 show the temporal and spatial variation of EVI (panel A), NDVI (panel B), and SAVI (panel C) across the whole observation period (2021-01 to 2022-08) for the three investigated fields, respectively.

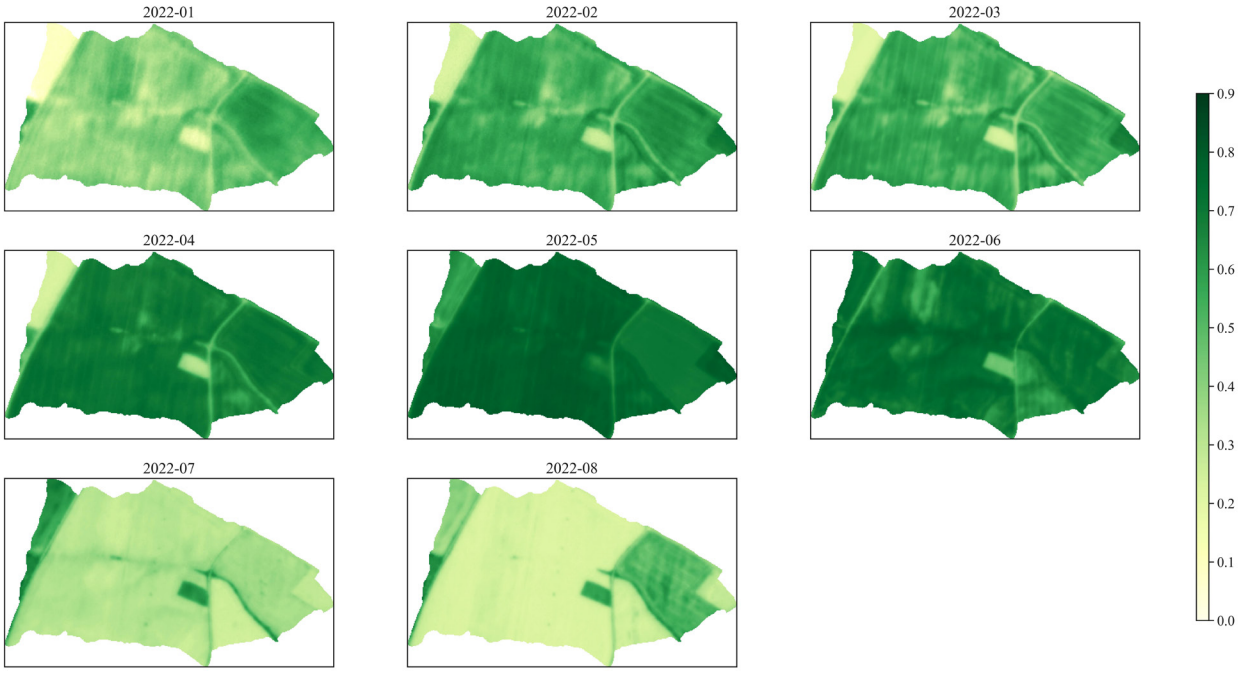

Figure 2. The monthly average of the normalised difference vegetation index (NDVI) value in 2022 across the catchment

https://doi.org/10.17221/60/2023-SWR

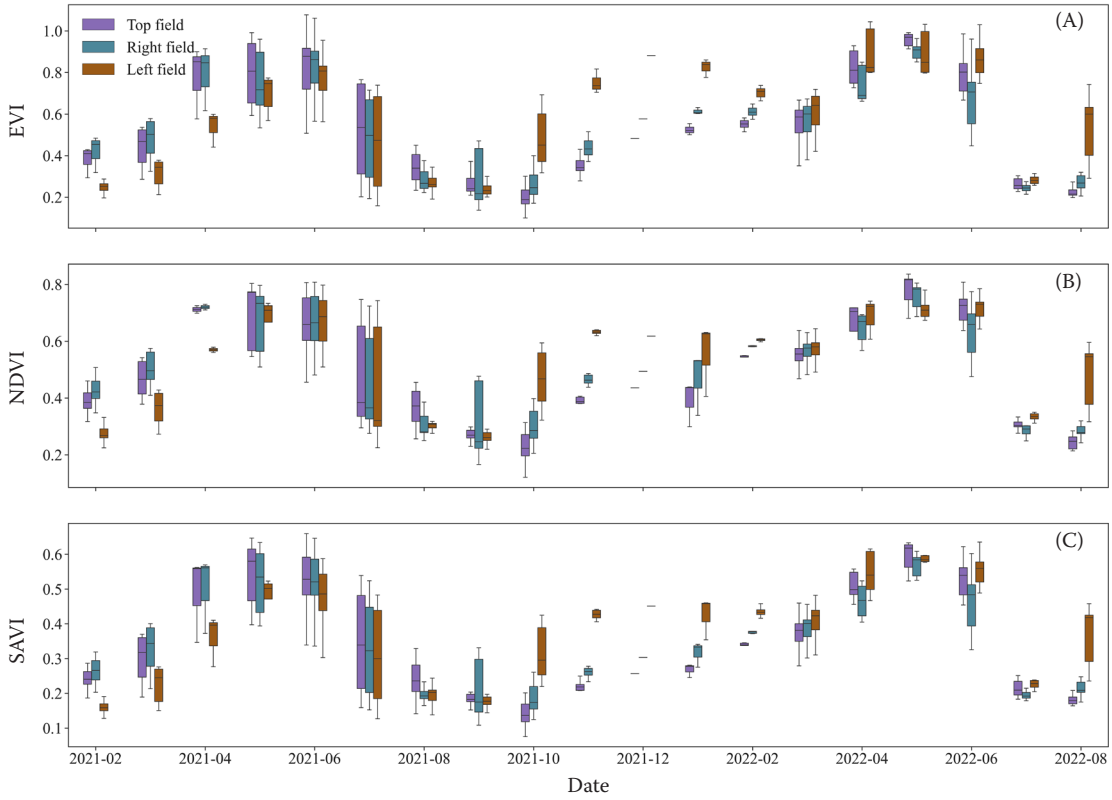

Figure 3. Temporal variation of the vegetation indices (VIs) across the three fields
EVI – enhanced vegetation index; NDVI – normalised difference vegetation index; SAVI – soil-adjusted vegetation index

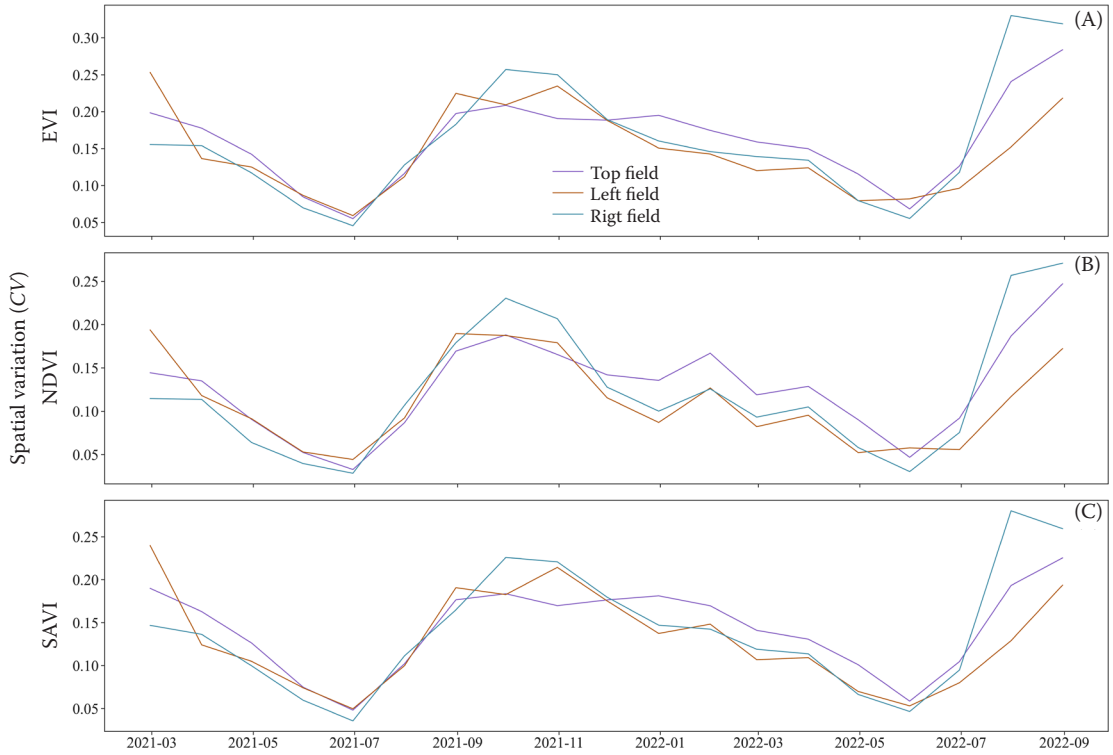

Figure 4. The coefficient of variation (*CV*) of the vegetation indices (VIs) fluctuates across three fields
EVI – enhanced vegetation index; NDVI – normalised difference vegetation index; SAVI – soil-adjusted vegetation index

https://doi.org/10.17221/60/2023-SWR

During the study period, there was a notable variability in the vegetation of the three fields (Figure 2). Moreover, all VIs followed the same temporal pattern: the highest values of VIs typically occurred during the spring and summer months (along with the highest variation ranges), whereas the lowest values and variation ranges of VIs typically occurred in autumn and winter due to crop harvesting and crop residue removal (Figure 3; Table 1). VIs are sensitive to various biophysical and biochemical parameters of vegetation, including biomass, leaf area index (LAI), photosynthetically active radiation (PAR), chlorophyll content, and water content (Hatfield & Prueger 2010; Kokhan & Vostokov 2020). The seasonal pattern of VIs observed in this study can be explained by the phenological stages of the crops and their responses to environmental conditions (Hatfield & Prueger 2010): higher values of VIs in spring and summer indicate higher biomass production, LAI expansion, chlorophyll synthesis, and PAR interception by the crops, lower values of VIs in autumn and winter indicate lower biomass production, LAI reduction, chlorophyll degradation, and PAR reflection by the crops or soil surface. The variation ranges of VIs also depend on the phenological stages: wider ranges occurred when crops were rapidly growing or harvested; narrower ranges appeared when crops were in early growing stages or already mature.

There were noticeable distinctions in all the VIs throughout the three fields (Figures 2, 3) due to differences (Table 1) in tillage practices and crop management (Noreika et al. 2020). Despite the fact that all three fields were assumed to be uniformly managed, spatial variation in VIs was observed in each field (Figure 2, 4). Spatial variations in VIs among all fields were observed to follow a similar seasonal trend in line with crop development. As the crops grew over the spring and summer, spatial variation steadily declined, reaching its lowest point when VIs achieved their highest values, suggesting that the crops were ripe and ready for harvest. Subsequently, spatial variance also gradually increased during autumn and winter after crop harvesting. This inverse relationship between the spatial variability (*CV*) of VIs and VIs values was consistent with previous findings (Martin et al. 2007; Chanda et al. 2018).

The spatial variation of VIs within each field can be attributed to several factors that affect soil-plant

Table 1. Crop information on each field from field cameras

Month	Top field	Left field	Right field
2021-04	mustard	wheat	mustard
2021-05	mustard	wheat	mustard
2021-06	mustard	wheat	mustard
2021-07	mustard	wheat	mustard
2021-08	1^{st}–7^{th} mustard 7^{th}–5^{th} crop residues after 15^{th} bare soil	1^{st}–8^{th} wheat 8^{th}–3^{rd} crop residues after 23^{rd} bare soil	bare soil
2021-09	bare soil	bare soil	bare soil
2021-10	no data	no data	wheat
2021-11	no data	no data	wheat
2021-12	no data	no data	wheat
2022-01	wheat	mustard	wheat
2022-02	wheat	mustard	wheat
2022-03	wheat	mustard	wheat
2022-04	wheat	mustard	wheat
2022-05	wheat	mustard	wheat
2022-06	wheat	mustard	wheat
2022-07	1^{st}–21^{st} wheat after 21^{st} crop residues	1^{st}–29^{th} mustard after 29^{th} crop residues	wheat (harvest between 14^{th}–27^{th}) after harvest: bare soil
2022-08	1^{st}–4^{th} crop residues after 4^{th} bare soil after 20^{th} cover crops	1^{st}–26^{th} crop residues after 26^{th} bare soil	bare soil

https://doi.org/10.17221/60/2023-SWR

interactions. For example, elevation can influence soil moisture availability and temperature gradients; soil characteristics can affect water-holding capacity, nutrient supply and root growth; slope can affect water runoff and erosion. Moreover, according to Jeřábek et al. (2022), slope-wise wheel tracks exhibited high structural connectivity and low roughness, increasing runoff and sediment transport. These consequences of slope-wise wheel tracks are also evident in our study (Figure 2), particularly in the top field: the values of the VIs were lower along the wheel tracks. In addition, landscape management change (large fields have been progressively subdivided into smaller fields in the Czech farmlands, see Noreika et al. (2021)) can also contribute to the spatial variance in each field varying over time (Figure 4). The spatial variation of VIs due to landscape management change can be understood as a consequence of altering the spatial distribution of crops and soil patches. For instance, subdividing large fields into smaller ones creates more edges and boundaries between different fields, which may increase or decrease contrast in VI values depending on crop types, management practices, and environmental conditions. Smaller fields may also have different hydrological regimes than larger ones, which affects plant growth and stress responses. According to previous studies (Noreika et al. 2021, 2022), field reductions in the Czech farmlands may strengthen the local water cycle and enhance water retention, which may lead to positive outcomes.

The mutual correlation among the VIs, ET and SWS. During the crop season (Table 1), the VIs at the soil moisture site PL144 followed the pattern EVI > NDVI > SAVI (Figure 5B), which indicates that EVI was more sensitive to vegetation changes than NDVI

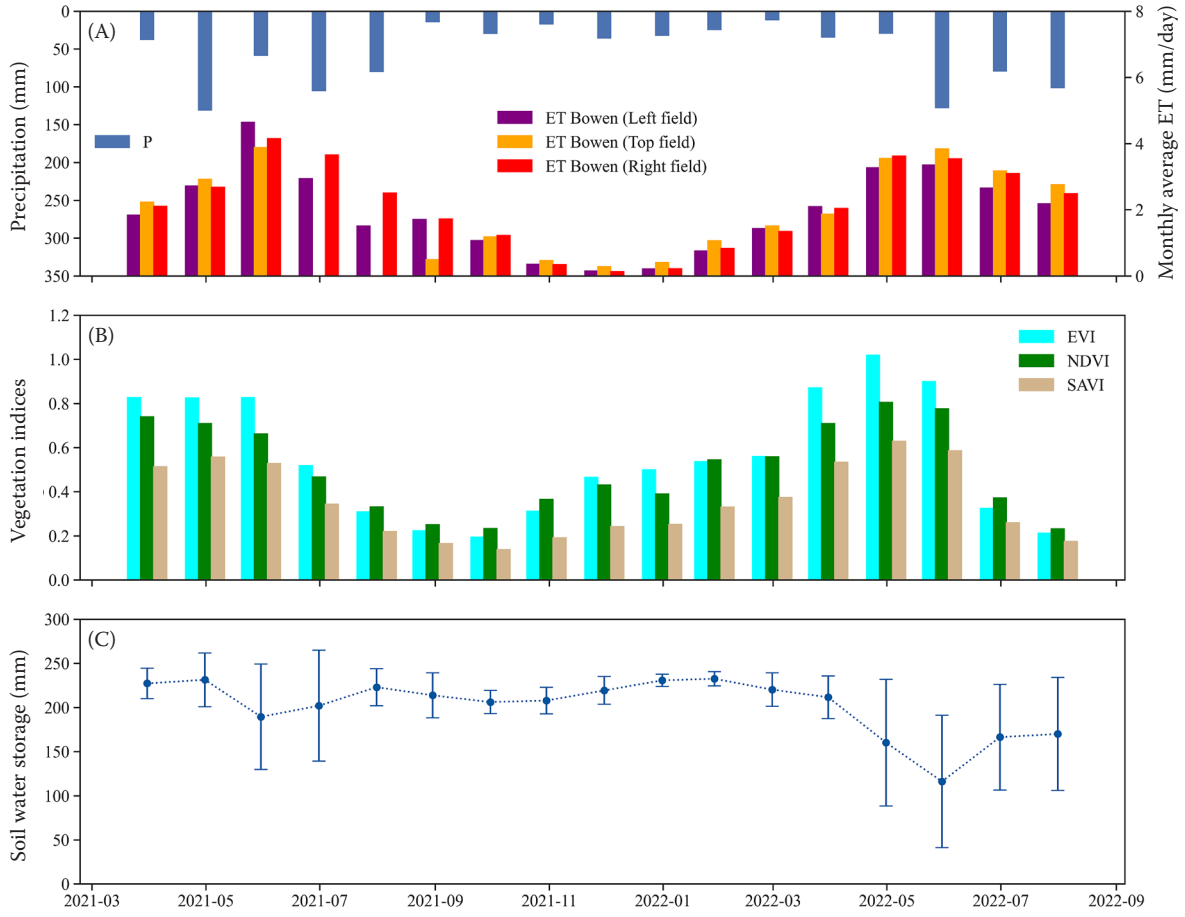

Figure 5. Temporal change of meteorological variables (precipitation and evapotranspiration (ET)) across the catchment (A), monthly average vegetation indices (B) and soil water storage (C) near soil moisture storage at site PL144
EVI – enhanced vegetation index; NDVI – normalised difference vegetation index; SAVI – soil-adjusted vegetation index; due to sensor failure, there were two months of data missing on the top field ET measurement

https://doi.org/10.17221/60/2023-SWR

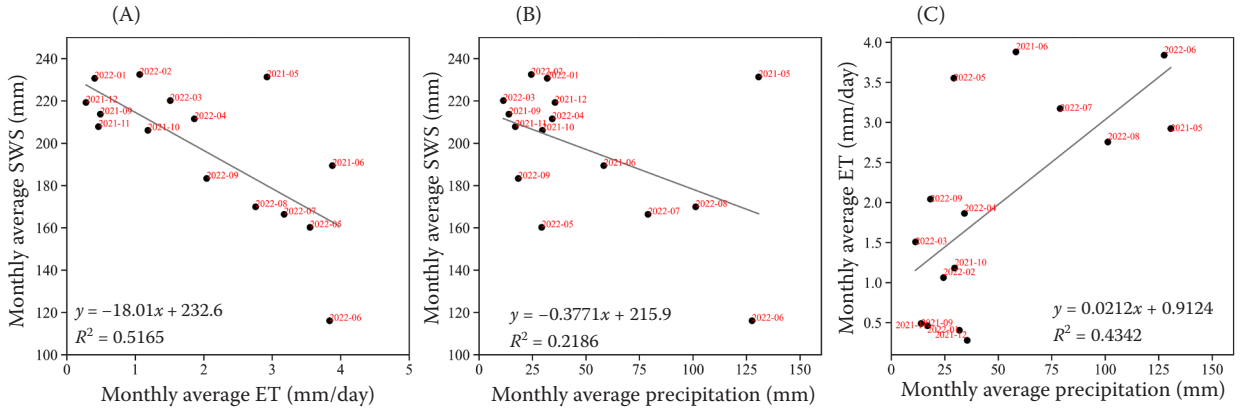

Figure 6. The mutual correlation between the monthly average soil water storage (SWS) and evapotranspiration (ET) rate from the top field (A), monthly average SWS and precipitation rate (B), monthly average precipitation rate and ET rate (C)

and SAVI (Huete et al. 2002). However, NDVI was higher than EVI when there was no or sparse vegetation, suggesting that NDVI was more influenced by soil reflectance than EVI (Huete et al. 2002). SAVI was lower than both NDVI and EVI throughout the year, implying that SAVI reduced the soil brightness contribution to VI values (Huete 1988).

The ET revealed a similar seasonal tendency with VIs (Figure 5A), with high ET rates (up to 5 mm/day) in the summer and low ET values (nearly 0) in the winter. ET is influenced by several vegetative properties, including the LAI and chlorophyll content, which explains this relationship. Specifically, summer months with high air temperatures and net radiation result in increased soil evaporation. Simultaneously, he presence of active vegetation with higher LAI and chlorophyll content increases plant transpiration and canopy interception, and hence higher levels of ET. In contrast, soil evaporation rates are reduced during the winter due to the cooler air temperature and decreased net radiation. Additionally, when vegetation is sparse, LAI and chlorophyll content are reduced, resulting in less plant transpiration and canopy interception and lower ET values. These findings highlight the importance of considering seasonal variations in vegetation characteristics in ET estimation and suggest that VIs can be a useful tool for predicting ET dynamics in different seasons (Glenn et al. 2010).

The seasonal pattern of SWS (Figure 5C) showed a high value in winter (up to 240 mm) and a low value in summer, with the lowest value (around 120 mm) occurring in June. Moreover, the SWS usually had considerable variations (about 150 mm) during the spring and summer months (from May to August). Regarding the climatic drivers of SWS, the correlation between SWS and monthly ET rate was stronger than that between SWS and monthly precipitation depth (Figure 6), suggesting that ET was the dominant factor influencing the monthly scale changes in SWS during the cropping season. This implies that crop water consumption had a more significant impact on soil moisture dynamics than the precipitation input during the growing season. These results emphasise the importance of considering both seasonal variations and crop water use when examining soil moisture dynamics.

Figures 7 and 8 illustrate the quantitative associations between monthly VIs, ET, and SWS during a single crop growth season (2021-08 to 2022-06). In addition, Table 2 quantified the fitted functions and their fit quality across all the variables.

The monthly VIs and ET (Figure 7) showed a similar seasonal pattern across all the fields: they were low in autumn and winter, when the crop was at the initial stage, and the soil moisture was high (Figures 5, 6), and then increased sharply in spring and summer, when the crop developed rapidly and needed more water for transpiration. This is consistent with previous studies that have used remote sensing data to monitor crop water use and stress at different spatial and temporal scales (Glenn et al. 2010).

However, the relationship between VIs and ET is not always linear but rather depends on various factors such as net radiation, temperature, soil moisture, and vegetation characteristics (Wang et al. 2007). For example, as demonstrated by various studies (Nguy-Robertson et al. 2014; Shafian et al. 2018; Bajocco et al. 2022; Ukasha et al. 2022), VIs and LAI

https://doi.org/10.17221/60/2023-SWR

in croplands, especially winter wheat, exhibit strong but non-linear relationships that can be modelled by an exponential function. Similarly, Nagler et al. (2013) developed an exponential model using MODIS-based EVI as a surrogate for LAI to estimate the actual evapotranspiration in riparian zones (Nagler et al. 2005, 2020). Abbasi et al. (2021) further adapted this exponential model to investigate the ET-VIs correlations for croplands at 30 m resolution and found good agreement with ground measurements. These studies suggest that VIs can be useful indicators of ET dynamics in different ecosystems, but they require site-specific calibration and validation.

Therefore, our study presented a simple method to reveal the ET-VIs relations across a single crop growing season by exponential functions. The correlation coefficients for the exponential functions between VIs and ET ranged from 0.6 to 0.9, depending on the field and the VI. The highest correlations were found for NDVI, which may be attributed to its sensitivity to green vegetation cover and chlorophyll content. In contrast, EVI showed the lowest correlations with ET, which may be due to its correction for soil and atmospheric effects, which further increases its sensitivity to vegetation changes (Abbasi et al. 2021; Huete et al. 2002). This approach is easy

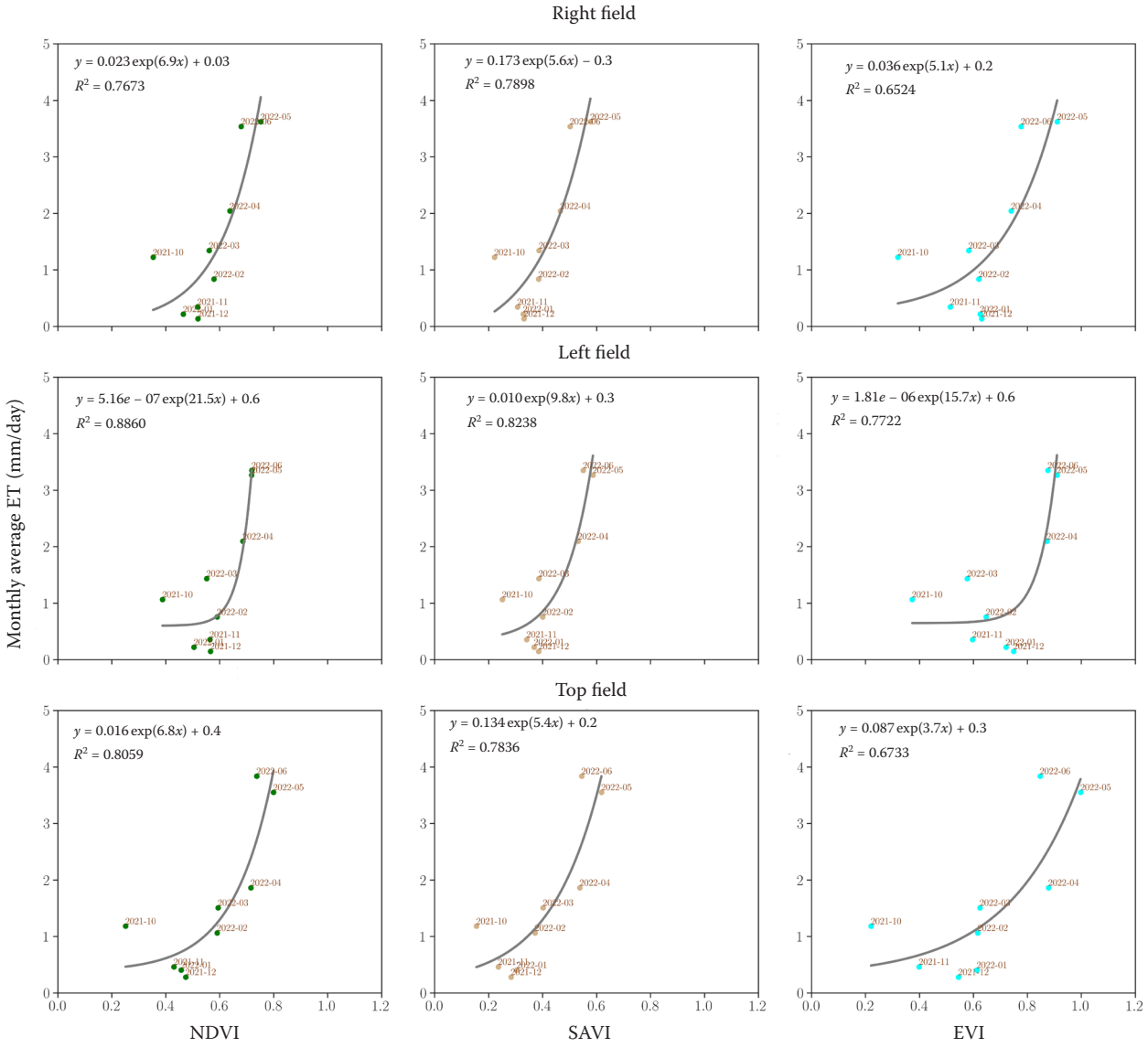

Figure 7. The correlation between monthly average vegetation indices (VIs) (around the evapotranspiration (ET) stations) and monthly average ET rate

NDVI – normalised difference vegetation index; SAVI – soil-adjusted vegetation index; EVI – enhanced vegetation index

https://doi.org/10.17221/60/2023-SWR

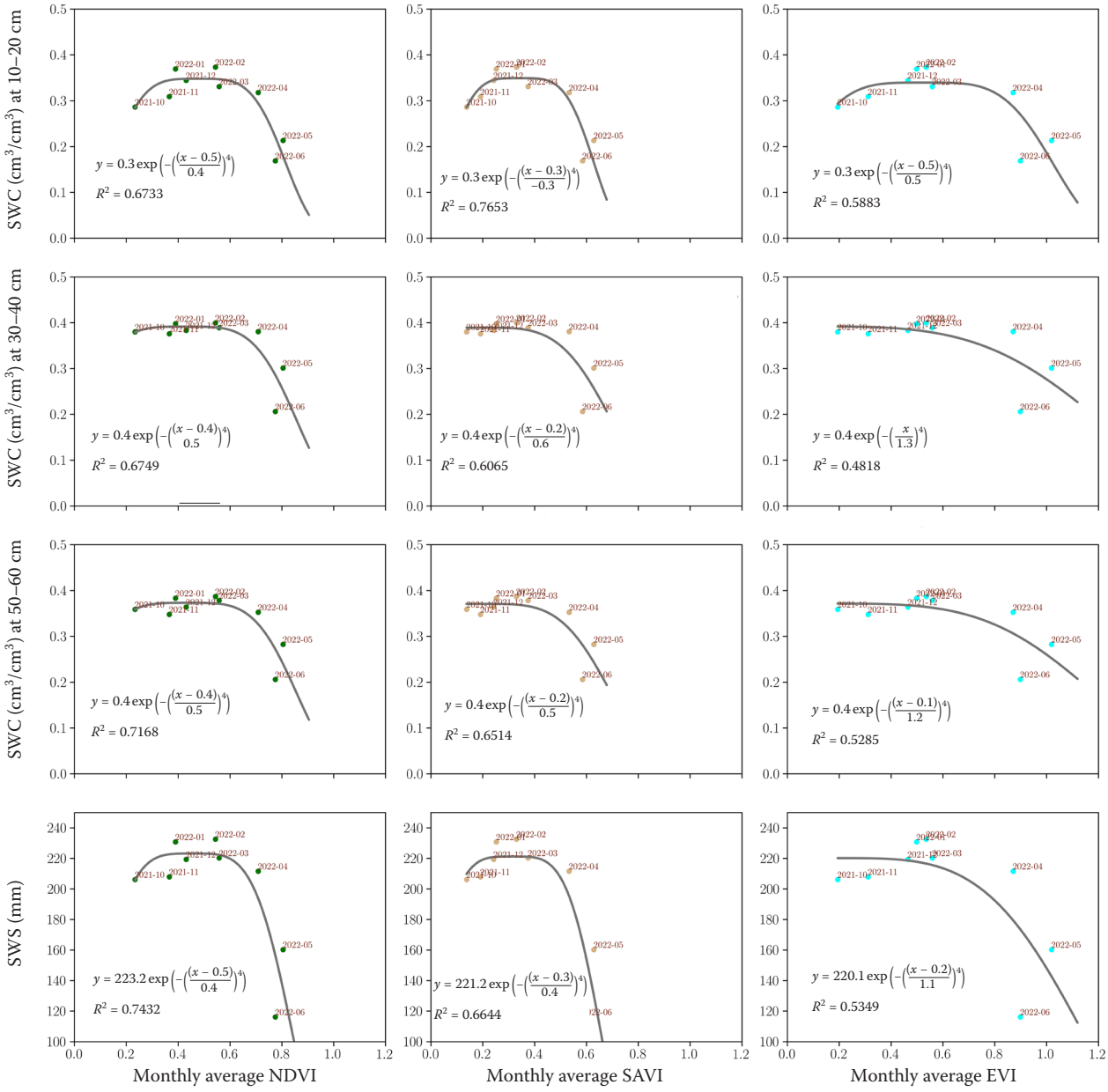

Figure 8. The correlation between monthly average VIs and monthly average soil water content at the soil moisture station PL144

EVI – enhanced vegetation index; NDVI – normalised difference vegetation index; SAVI – soil-adjusted vegetation index; SWS – soil water storage; SWC – soil water content

to understand and use, making it ideal for areas with restricted water resources and limited ground data. It simply needs affordable and widely available optical satellite data and meteorological data. The non-linear relationship between VIs and ET can also be captured, which is reflective of crop growth and water demands. Moreover, it can provide reliable estimates of ET at high spatial resolution (3 m), which can capture the heterogeneity of crop water demands in croplands. Nevertheless, this method cannot be applicable to other seasons, as it is calibrated only for the growing season. Furthermore, the quality and accuracy of satellite and meteorological data and the translation and localisation of VIs across multiple sensors may contribute to inaccuracies and uncertainties. Therefore, it is crucial to validate and calibrate this method with ground measurements of meteorological data and compare it with

https://doi.org/10.17221/60/2023-SWR

other methods that use different data sources (e.g. thermal-based, hydrological modelling).

The soil water storage also showed a clear seasonal pattern with VIs (Figure 8), but with an opposite trend. Specifically, the soil water storage was high and stable in autumn and winter, when the ET was low, and the precipitation exceeded the crop water demand. Then, the soil water storage dropped sharply in spring and summer when the evapotranspiration increased with the crop growth, and the precipitation was insufficient to replenish the soil water storage. Furthermore, our results suggest that VIs were more strongly associated with soil moisture in the uppermost layer of soil than in deeper layers. This finding indicates that VIs primarily reflected soil moisture conditions in the topsoil, which is directly affected by surface vegetation conditions, such as leaf area index (LAI), canopy cover, and root zone depth (Li et al. 2022; Stocker et al. 2023). Seasonal changes in precipitation and temperature can also influence soil moisture in this layer. In contrast, deeper soil layers are less influenced by surface vegetation but

Table 2. Fitted exponential functions among all the variables

Variables *X*	Variables *Y*	Exponential function	RMSE	R^2
NDVI	T_ET	$Y = 0.016e^{6.8X} + 0.4$	0.546	0.8059
	R_ET	$Y = 0.023e^{6.9X} + 0.03$	0.609	0.7673
	L_ET	$Y = 5.16e - 7e^{21.5X} + 0.6$	0.395	0.8860
	SWC_10 cm	$Y = 0.3e^{-\left(\frac{X-0.5}{0.4}\right)^4}$	0.028	0.8145
	SWC_30 cm	$Y = 0.4e^{-\left(\frac{X-0.4}{0.5}\right)^4}$	0.034	0.6749
	SWC_60 cm	$Y = 0.4e^{-\left(\frac{X-0.4}{0.5}\right)^4}$	0.030	0.7168
	SWS	$Y = 223.1e^{-\left(\frac{X-0.5}{0.4}\right)^4}$	18.21	0.7432
SAVI	T_ET	$Y = 0.134e^{5.4X} + 0.2$	0.576	0.7836
	R_ET	$Y = 0.173e^{5.6X} - 0.3$	0.578	0.7898
	L_ET	$Y = 0.010e^{9.8X} + 0.3$	0.492	0.8238
	SWC_10 cm	$Y = 0.3e^{-\left(\frac{X-0.3}{0.3}\right)^4}$	0.032	0.7653
	SWC_30 cm	$Y = 0.4e^{-\left(\frac{X-0.2}{0.6}\right)^4}$	0.037	0.6065
	SWC_60 cm	$Y = 0.4e^{-\left(\frac{X-0.2}{0.5}\right)^4}$	0.033	0.6514
	SWS	$Y = 221.2e^{-\left(\frac{X-0.3}{0.4}\right)^4}$	20.82	0.6644
EVI	T_ET	$Y = 0.087e^{3.7X} + 0.3$	0.708	0.6733
	R_ET	$Y = 0.036e^{5.1X} + 0.2$	0.744	0.6524
	L_ET	$Y = 1.81e - 6e^{15.7X} + 0.6$	0.559	0.7722
	SWC_10 cm	$Y = 0.3e^{-\left(\frac{X-0.5}{0.5}\right)^4}$	0.042	0.5883
	SWC_30 cm	$Y = 0.4e^{-\left(\frac{X}{1.3}\right)^4}$	0.043	0.4818
	SWC_60 cm	$Y = 0.4e^{-\left(\frac{X-0.1}{1.2}\right)^4}$	0.038	0.5285
	SWS	$Y = 220.1e^{-\left(\frac{X-0.2}{1.1}\right)^4}$	24.52	0.5349

EVI – enhanced vegetation index; NDVI – normalised difference vegetation index; SAVI – soil-adjusted vegetation index; ET – evapotranspiration; SWC – soil water storage; RMSE – root mean square error

https://doi.org/10.17221/60/2023-SWR

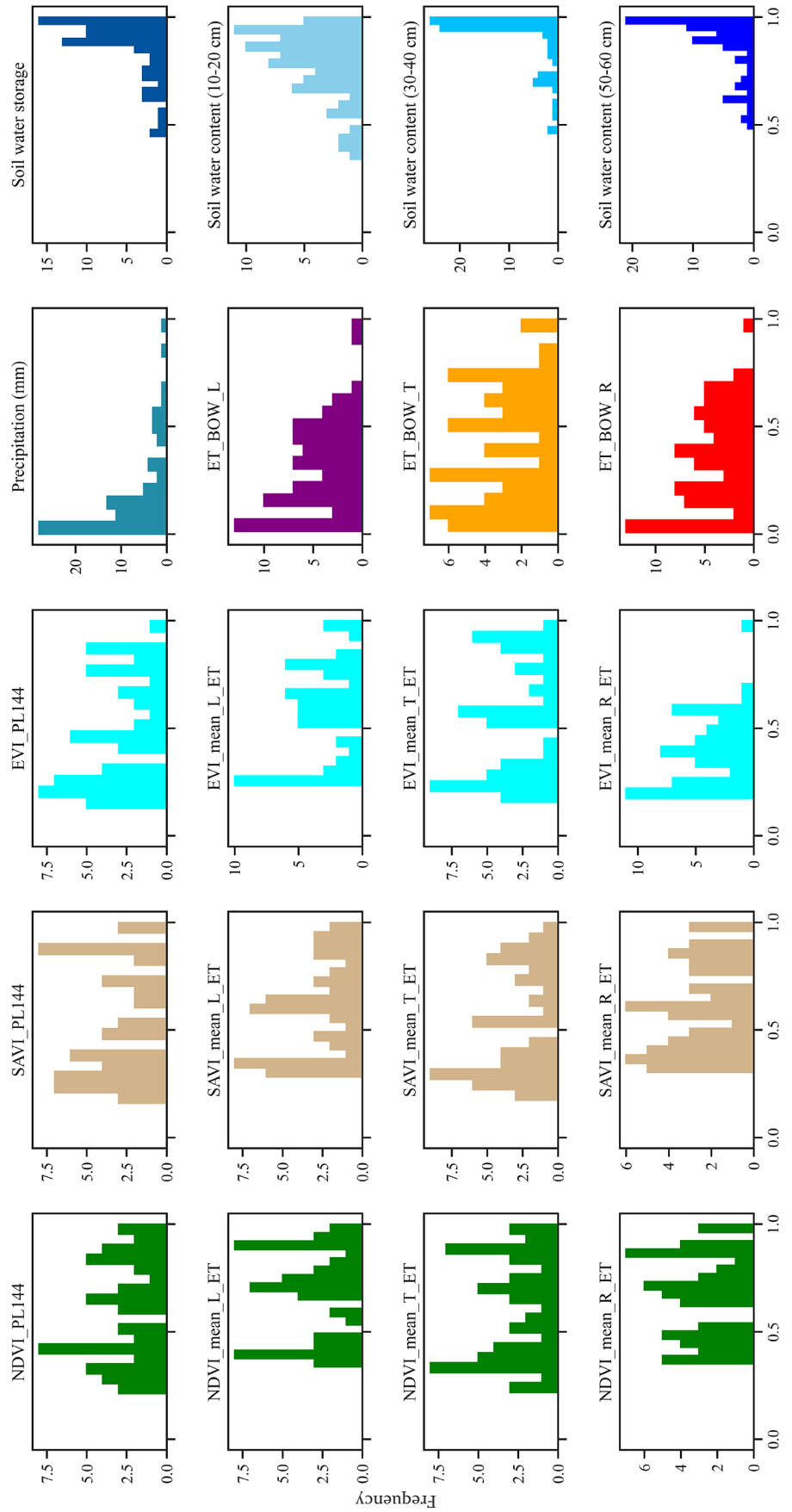

Figure 9. Distribution of the normalised variables
NDVI – normalised difference vegetation index; SAVI – soil-adjusted vegetation index; EVI – enhanced vegetation index; ET – evapotranspiration; L – left field; R – rigt field; T – top field

https://doi.org/10.17221/60/2023-SWR

more by subsurface hydrological processes, such as percolation and drainage (Trautmann et al. 2022). As a result, the soil water content in these layers may be more stable over time unless there are extreme events. However, it is important to note that the relationship between soil water storage and VIs may vary depending on vegetation type and climate conditions. For example, previous studies have reported that SWS and VIs are positively correlated in grasslands, shrublands and forestlands, where deep-rooted plants can access water stored in deeper soil layers or groundwater (Fan et al. 2017; Zhang et al. 2021; Stocker et al. 2023). In contrast, other studies have found that SWS and VIs are negatively correlated in areas where shallow-rooted plants were planted, as they rely on topsoil moisture and are sensitive to water stress (Wang et al. 2007; Cao et al. 2018).

Seasonal variations in the VIs, ET, and SWS. Figure 9 presents the seasonal distribution of all normalised variables investigated in the analysis. Most fields demonstrated a right-skewed distribution pattern for evapotranspiration (except for the top field, ET_BOW_T) and precipitation, implying that high ET and extreme precipitation rates are uncommon across all the fields. In contrast, soil water storage and soil water content in the root zone displayed left-skewed distribution patterns, indicating that the soil is mostly under wet conditions. For the vegetation indices, multimodal distributions of NDVI, SAVI, and EVI were observed at all stations.. Notably, the EVI demonstrated a tendency towards a positively-skewed distribution, which is similar to the evapotranspiration distribution, in contrast to the left-skewed distributions observed for soil water storage.

An appraisal of statistical moments variation on a seasonal basis for each variable can provide information concerning (*i*) how quantities are mutually related and (*ii*) which might be coupled hence being mutually employed for describing the variation of each other. The present analysis, again, was split into three parts, each one for each field under consideration.

The distribution patterns inferred both from Figures 9 and 10 lead us to consider how well the seasonal soil moisture dynamics, here resembled by SWS, might be related to vegetation indices or vice-versa. In this case, unknown soil moisture content would be surrogated, at least for the moments of the distribution, by those of vegetation patterns.

Each panel of Figure 10 suggests that the VIs are more closely related to SWS seasonal variations than to precipitation inferred from available gauges based on their mean seasonal values. This finding

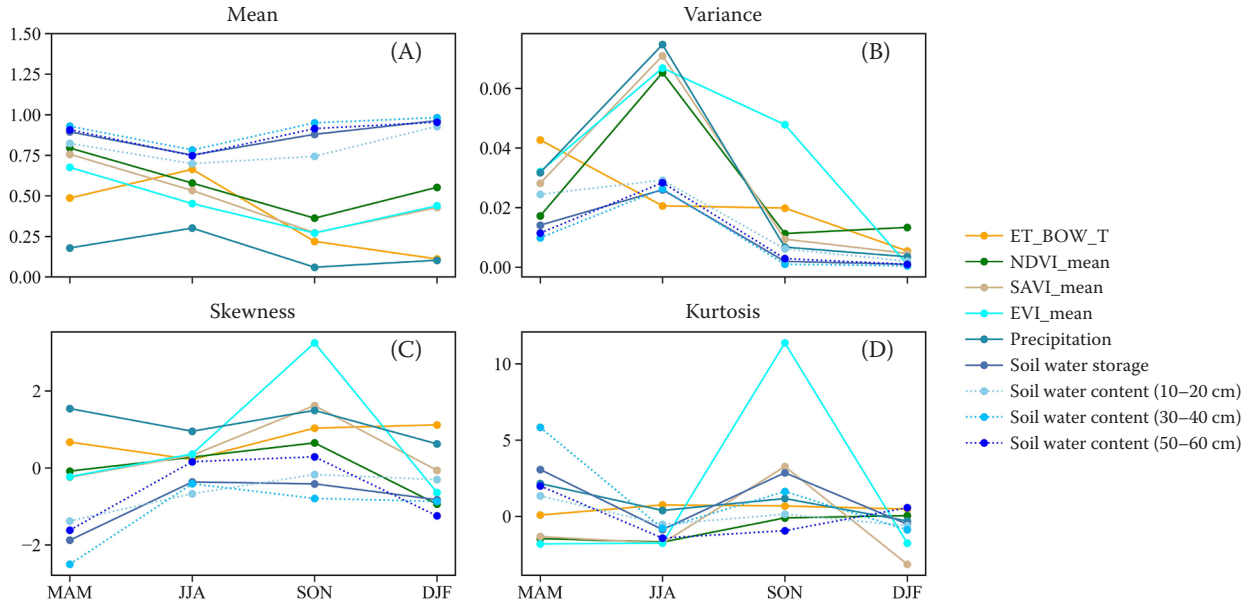

Figure 10. Statistical moments of the variables at the upper field (PL144 station)
MAM – the spring months (March, April, May); JJA – the summer months (June, July, August); SON – the autumn months (September, October, November); DJF – the winter months (December, January, February); ET – evapotranspiration; NDVI – normalised difference vegetation index; SAVI – soil-adjusted vegetation index; EVI – enhanced vegetation index

https://doi.org/10.17221/60/2023-SWR

is highly instructive, as it emphasises the importance of assessing subsurface flow patterns to properly understand crop growth and vegetation indices' spatial distribution, as previously noted by Schiavo (2022). It is worth noting that while SWS has the same temporal behaviour as VIs (e.g., decreases in summer), precipitation behaves differently and may not be directly related to crop vegetation indices.

Our analysis revealed that SWS exhibits considerable differences from other variables when examining higher moments (k = 3, 4) of seasonal values' distributions, which is evident from all the panels investigated. Here two considerations must be highlighted. First, we note that SWS and ET have a similar seasonal trend, even though their seasonal values are very different. We think that this similarity is enough to show some relation between these variables for higher orders of distribution, and to keep SWS relevant for our discussion. Second, skewness and kurtosis (Kendall & Stuart 1969; Sharma & Bhandari 2015; Schiavo et al. 2022) are employable to inform about patterns of the distribution itself (i.e. its asymmetry (right/left skew) or its flatness, respectively) rather than for a quantitative comparison. For the latter purpose, mean and variance are more suitable to capture our seasonal values' variation. Furthermore, skewness and kurtosis between different variables) can help us compare the qualitative aspects of different variables' distributions, for example if they share a similar tendency to flatten on a particular season or not. This is the purpose why we employed them, as well as Schiavo (2022) did with a precise type of distribution whose skewness and kurtosis are relevant traits.

Employing the NNSE index (Normalised Nash-Sutcliffe Index) upon ET and soil water storage as dependent variables helps assess the relationship between these variables and other dependent ones. Moreover, these indices are seasonally organised to identify if any temporal patterns arise from this analysis. When evaluating the relationship between ET or SWS and other variables, it is essential to consider both the median estimated NNSE and its range of variation. These values can significantly vary from season to season, and it is important to remember the regional climate patterns in the Czech Republic, which has drier springs and winters but wet summers and autumns due to its Continental Climate type (Hanel et al. 2013).

Figure 12 illustrate the relationship between ET (employed as an independent variable) with mean precipitation rate and VIs (NDVI, SAVI, EVI, respectively) for each field (employed as dependent variables). Their seasonal patterns are quite comparable and can be discussed jointly. NNSE values, computed across all the seasons and fields, indicate that precipitation has the highest seasonal similarity with ET compared to other variables. This finding aligns with the strong correlation observed between monthly ET and precipitation rate (Figure 6) and the similarity of their distributions (Figure 9). Precipitation has high consistency with ET because the amount of precipitation largely determines the amount of water available for ET, which directly affects the ET rate. When there is more precipitation, there is more water available for ET, leading to an increase in the ET rate. Similarly, when there is less precipitation, the amount of water available for ET decreases, resulting in a decrease in the ET rate. This is why there is a strong correlation between monthly ET and precipitation rate, as well as a similarity in their distributions. However, among all the seasons, the precipitation has the highest NNSE in spring and autumn, with a slight decrease in summer, potentially influenced by the growing vegetation. The lowest NNSE values appeared in winter, indicating the lowest consistency between precipitation and ET during this season. This can be attributed to winter precipitation falling as snow, which can accumulate on the ground, limiting water availability for ET.

Regarding the seasonal similarity between ET and VIs, all the VIs demonstrate comparable values across all seasons. However, EVI shows slightly higher similarity than NDVI and SAVI, which may be attributed to its higher sensitivity to changes in vegetation cover, as previously reported by Huete et al. (2002). In terms of seasonality, the similarity between ET and VIs gradually increases from winter to summer, reaching the highest values in summer. Then it drops sharply in autumn (with the highest variation) to the lowest value in winter (also revealed in the differences in statistical moments in Figure 11).

Moreover, among all the seasons, the top field showed slightly higher NNSE values than the other two fields. We hypothesise that these differences in seasonal efficiency could be due to the differences in topography and size between the fields. Specifically, the top field is the largest field and has the highest elevation and distance from the outlet, while the other two fields are less than half its size and adjacent to the main surface outflow channel. Therefore, the most elevated (top) field would accumulate

https://doi.org/10.17221/60/2023-SWR

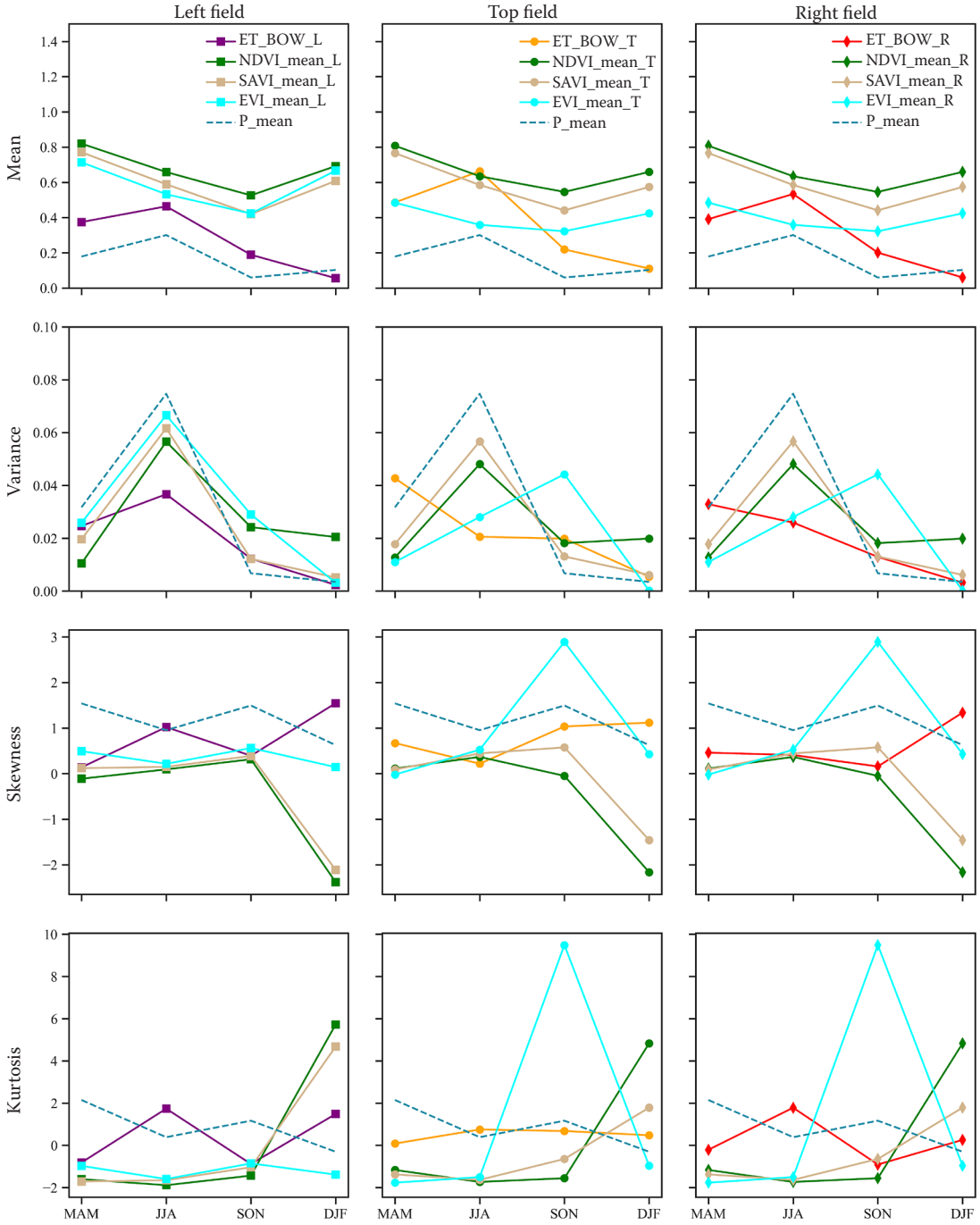

Figure 11. Statistical moments of the variables

Evapotranspiration (ET) calculated from Bowen ratio: ET_BOW_X; VIs: NDVI/SAVI/EVI_mean_X; precipitation: P_mean_X (X stands for the field) at three fields (L: left field; R: right field; T: Top field)

MAM – the spring months (March, April, May); JJA – the summer months (June, July, August); SON – the autumn months (September, October, November); DJF – the winter months (December, January, February); NDVI – normalised difference vegetation index; SAVI – soil-adjusted vegetation index; EVI – enhanced vegetation index

infiltration during wet seasons while subsequently releasing part of its storage through the subsurface during dry seasons, affecting its soil water storage and ET potential. This way, the top field's ET (Figure 12B) and soil water storage (Figure 13) would be strongly influenced by seasonal rainfall, while the down-

https://doi.org/10.17221/60/2023-SWR

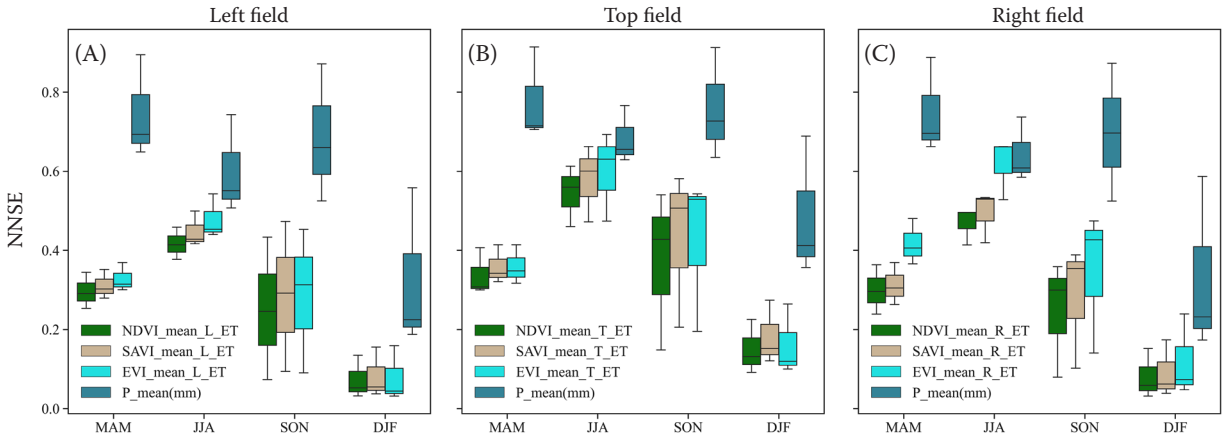

Figure 12. Normalised Nash-Sutcliffe index (NNSE) of the variables against evapotranspiration (ET) values from three ET stations
MAM – the spring months (March, April, May); JJA – the summer months (June, July, August); SON – the autumn months (September, October, November); DJF – the winter months (December, January, February); NDVI – normalised difference vegetation index; SAVI – soil-adjusted vegetation index; EVI – enhanced vegetation index; P – precipitation

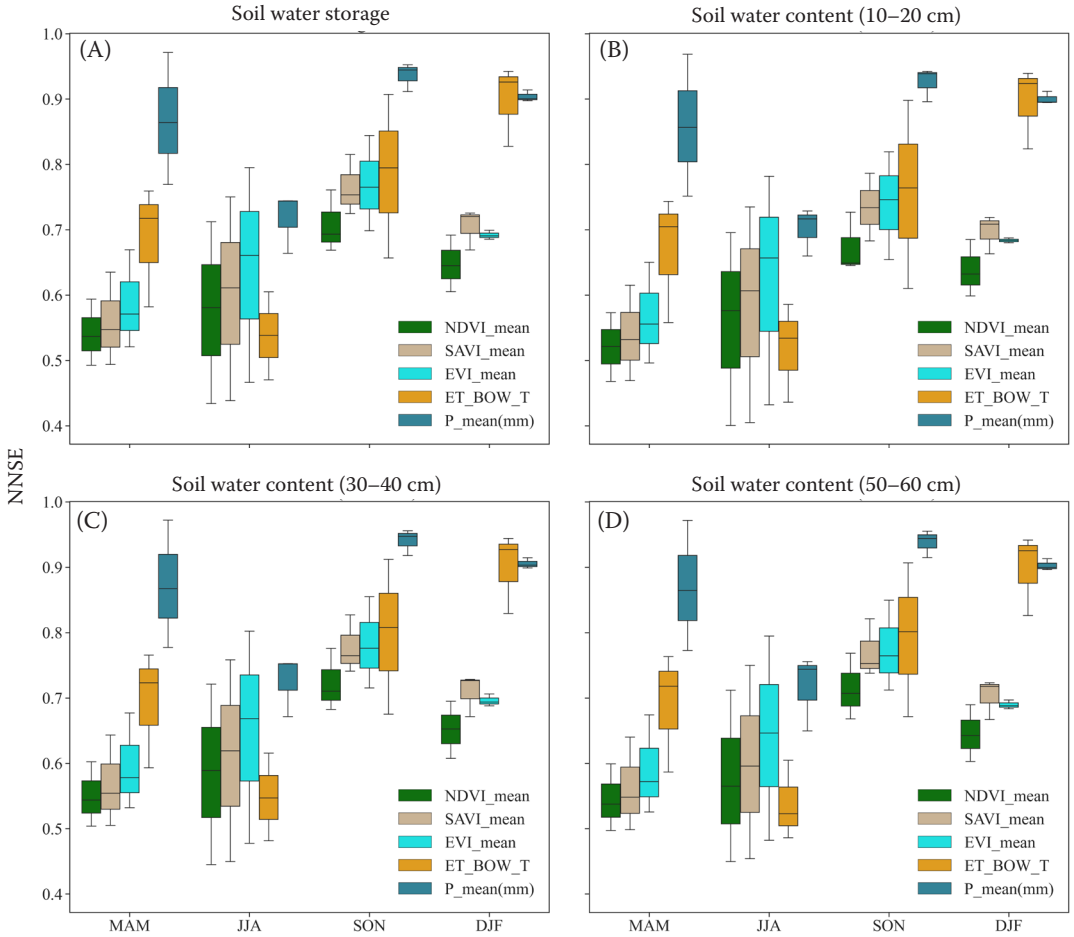

Figure 13. Normalised Nash-Sutcliffe index (NNSE) of the variables against soil moisture measurement from the soil water storage (SWS) PL144 station
MAM – the spring months (March, April, May); JJA – the summer months (June, July, August); SON – the autumn months (September, October, November); DJF – the winter months (December, January, February); NDVI – normalised difference vegetation index; SAVI – soil-adjusted vegetation index; EVI – enhanced vegetation index; ET – evapotranspiration; P – precipitation

https://doi.org/10.17221/60/2023-SWR

stream fields would be far less sensitive to infiltration seasonal variations, being recharged through the subsurface by their upper neighbour. Consequently, the top field's highest NNSE values would be during the summer season, with high variation ranges due to changes in precipitation. Accordingly, the top field's subsurface storage would be higher during wet seasons, leading to a wetting front within the subsurface moving towards the surface outlet. This result suggests that both soil storage conditions and fields' sensitivity to recharge (e.g., infiltration) are influenced by subsurface morphology, which in our case seems to be similar to the surface topography. This finding is consistent with analyses performed at larger scales (Schiavo 2022; Schiavo et al. 2022) and provides a basis for further analysis.

The analysis of efficiency indices can provide insights on the interrelationships between the soil water content (employed as an independent variable) at varying depths within the root zone (10–20, 30–40, and 50–60 cm, respectively), estimated evapotranspiration via Bowen Ratio, and precipitation, as well as VIs, , across different seasons (Figure 13). From panels A–D, we can barely appraise a narrower range of variation of efficiency between vegetation indices and SWS integrated along the vertical (panel A), with that at increasing depths (panels from B to D), particularly in summer. On the contrary, the variation of efficiency between precipitation and increasing-depths soil water content widens, again, particularly in summer. While the former can be related to varying drying conditions during summer, hence soil water content is more related to vegetation indices for surficial soil layers, and the latter can be related to the infiltration of precipitation, returning slightly lower efficiency indices between deeper soil contents and precipitation. These considerations strengthen our ability to relate different hydrological processes to NNSE mutual efficiency and give hints about which variables might be more mutually correlated during a certain season.

CONCLUSION

In this study, we aimed to evaluate the evapotranspiration (ET) of a small agricultural catchment using various datasets, including high-resolution satellite images, precipitation, vegetation indices (VIs), and soil water storage (SWS). Our findings suggest a consistent seasonal trend in the variation of VIs across all fields, with the highest values recorded in spring and summer, and the lowest in autumn and winter due to crop harvesting and sparse vegetation. The correlation between ET, SWS, and VIs was also found to be strong, with exponential functions expressing their correlation within a crop growing season. We suggest that VIs may be useful in inferring ET or SWS, especially where it is poorly monitored. Additionally, our results indicate that the subsurface recharge may play a critical role in the water balance of the fields we investigated, and it is likely influenced by potential gradients of the water table and bedrock morphology. Overall, our study provides insights into the ET dynamics of a small agricultural catchment and highlights the importance of considering multiple variables in water resource management. Nonetheless, we only analysed the SWS dynamic from a single field, and we only investigated the intercorrelation between variables for a one crop season. Thus, future research should examine the SWS from various locations within the catchment and gather data from multiple crop growing seasons. In addition, future studies should focus on the spatial variability of ET and SWS at a field scale using high-resolution satellite images and other pertinent datasets.

REFERENCES

Abbasi N., Nouri H., Didan K., Barreto-Muñoz A., Chavoshi Borujeni S., Salemi H., Opp C., Siebert S., Nagler P. (2021): Estimating actual evapotranspiration over croplands using Vegetation Index methods and dynamic harvested area. Remote Sensing, 13: 5167.

Abowarda A.S., Bai L., Zhang C., Di Long, Li X., Huang Q., Sun Z. (2021): Generating surface soil moisture at 30 m spatial resolution using both data fusion and machine learning toward better water resources management at the field scale. Remote Sensing of Environment, 255: 112301.

Allen R.G., Pereira L.S., Raes D., Smith M. (1998): Crop Evapotranspiration-Guidelines for Computing Crop Water Requirements. FAO Irrigation and Drainage Paper No. 56. Rome, FAO.

Allen R.G., Pereira L.S., Howell T.A., Jensen M.E. (2011a): Evapotranspiration information reporting: I. Factors governing measurement accuracy. Agricultural Water Management, 98: 899–920.

Allen R.G., Pereira L.S., Howell T.A., Jensen M.E. (2011b): Evapotranspiration information reporting: II. Recommended documentation. Agricultural Water Management, 98: 921–929.

https://doi.org/10.17221/60/2023-SWR

Angus D.E., Watts P.J. (1984): Evapotranspiration — How good is the Bowen ratio method? Agricultural Water Management, 8: 133–150.

Aragon B., Houborg R., Tu K., Fisher J.B., McCabe M. (2018): CubeSats Enable high spatiotemporal retrievals of crop-water use for precision agriculture. Remote Sensing, 10: 1867.

Aragon B., Ziliani M.G., Houborg R., Franz T.E., McCabe M.F. (2021): CubeSats deliver new insights into agricultural water use at daily and 3 m resolutions. Scientific Reports, 11: 1–12.

Bajocco S., Ginaldi F., Savian F., Morelli D., Scaglione M., Fanchini D., Raparelli E., Bregaglio S.U.M. (2022): On the use of NDVI to estimate LAI in field crops: Implementing a conversion equation library. Remote Sensing, 14: 3554.

Baldocchi D.D. (2003): Assessing the eddy covariance technique for evaluating carbon dioxide exchange rates of ecosystems: Past, present and future. Global Change Biology, 9: 479–492.

Benninga H.J.F., van der Velde R., Su Z. (2022): Soil moisture content retrieval over meadows from Sentinel-1 and Sentinel-2 data using physically based scattering models. Remote Sensing of Environment, 280: 113191.

Biswas A. (2019): Joint multifractal analysis for three variables: Characterizing the effect of topography and soil texture on soil water storage. Geoderma, 334: 15–23.

Bogena H.R., Herbst M., Huisman J.A., Rosenbaum U., Weuthen A., Vereecken H. (2010): Potential of wireless sensor networks for measuring soil water content variability. Vadose Zone Journal, 9: 1002–1013.

Bowen I.S. (1926): The ratio of heat losses by conduction and by evaporation from any water surface. Physical Review, 27: 779–787.

Cao R., Jia X., Huang L., Zhu Y., Wu L., Shao M. (2018): Deep soil water storage varies with vegetation type and rainfall amount in the Loess Plateau of China. Scientific Reports, 8: 12346.

Chanda S., Kanke Y., Dalen M., Hoy J., Tubana B. (2018): Coefficient of variation from vegetation index for sugarcane population and stalk evaluation. Agrosystems, Geosciences & Environment, 1: 1–9.

Cheng M., Jiao X., Liu Y., Shao M., Yu X., Bai Y.,Wang Z., Wang S., Tuohuti N., Liu S., Shi L., Yin D., Huang X., Nie C., Jin X. (2022a): Estimation of soil moisture content under high maize canopy coverage from UAV multimodal data and machine learning. Agricultural Water Management, 264: 107530.

Cheng M., Li B., Jiao X., Huang X., Fan H., Lin R., Liu K. (2022b): Using multimodal remote sensing data to estimate regional-scale soil moisture content: A case study of Beijing, China. Agricultural Water Management, 260: 107298.

Cheng Y., Vrieling A., Fava F., Meroni M., Marshall M., Gachoki S. (2020): Phenology of short vegetation cycles in a Kenyan rangeland from PlanetScope and Sentinel-2. Remote Sensing of Environment, 248: 112004.

Cholpankulov E.D., Inchenkova O.P., Paredes P., Pereira L.S. (2008): Cotton irrigation scheduling in central Asia: Model calibration and validation with consideration of groundwater contribution. Irrigation and Drainage, 57: 516–532.

Crow W.T., Kustas W.P., Prueger J.H. (2008): Monitoring root-zone soil moisture through the assimilation of a thermal remote sensing-based soil moisture proxy into a water balance model. Remote Sensing of Environment, 112: 1268–1281.

Devitt D.A., Sala A., Smith S.D., Cleverly J., Shaulis L.K., Hammett R. (1998): Bowen ratio estimates of evapotranspiration for *Tamarix ramosissima* stands on the Virgin River in southern Nevada. Water Resources Research, 34: 2407–2414.

Estes L.D., Ye S., Song L., Luo B., Eastman J.R., Meng Z., Zhang Q., McRitchie D., Debats S.R., Muhando J., Amukoa A.H., Kaloo B.W., Makuru J., Mbatia B.K., Muasa I.M., Mucha J., Mugami A.M., Mugami J.M., Muinde F.W., Mwawaza F.M., Ochieng J., Oduol C.J., Oduor P., Wanjiku T., Wanyoike J.G., Avery R.B., Caylor K.K. (2022): High resolution, annual maps of field boundaries for smallholder-dominated croplands at national scales. Frontiers in Artificial Intelligence, 4: 164.

Famiglietti J.S., Rudnicki J.W., Rodell M. (1998): Variability in surface moisture content along a hillslope transect: Rattlesnake Hill, Texas. Journal of Hydrology, 210: 259–281.

Fan Y., Miguez-Macho G., Jobbágy E.G., Jackson R.B., Otero-Casal C. (2017): Hydrologic regulation of plant rooting depth. Proceedings of the National Academy of Sciences of the United States of America, 114: 10572–10577.

Fisher J.B., Tu K.P., Baldocchi D.D. (2008): Global estimates of the land–atmosphere water flux based on monthly AVHRR and ISLSCP-II data, validated at 16 FLUXNET sites. Remote Sensing of Environment, 112: 901–919.

Gao X. (2000): Optical–biophysical relationships of vegetation spectra without background contamination. Remote Sensing of Environment, 74: 609–620.

Gitelson A.A., Kaufman Y.J., Merzlyak M.N. (1996): Use of a green channel in remote sensing of global vegetation from EOS-MODIS. Remote Sensing of Environment, 58: 289–298.

Glenn E.P., Nagler P.L., Huete A.R. (2010): Vegetation index methods for estimating evapotranspiration by remote sensing. Surveys in Geophysics, 31: 531–555.

Granier A. (1987): Evaluation of transpiration in a Douglas-fir stand by means of sap flow measurements. Tree Physiology, 3: 309–320.

https://doi.org/10.17221/60/2023-SWR

Hanel M., Mrkvičková M., Máca P., Vizina A., Pech P. (2013): Evaluation of simple statistical downscaling methods for monthly regional climate model simulations with respect to the estimated changes in runoff in the Czech Republic. Water Resources Management, 27: 5261–5279.

Hatfield J.L., Prueger J.H. (2010): Value of using different vegetative indices to quantify agricultural crop characteristics at different growth stages under varying management practices. Remote Sensing, 2: 562–578.

He M., Kimball J.S., Yi Y., Running S.W., Guan K., Moreno A., Wu X., Maneta M. (2019): Satellite data-driven modeling of field scale evapotranspiration in croplands using the MOD16 algorithm framework. Remote Sensing of Environment, 230: 111201.

Hébrard O., Voltz M., Andrieux P., Moussa R. (2006): Spatio-temporal distribution of soil surface moisture in a heterogeneously farmed Mediterranean catchment. Journal of Hydrology, 329: 110–121.

Houborg R., McCabe M.F. (2018): Daily retrieval of NDVI and LAI at 3 m resolution via the fusion of CubeSat, Landsat, and MODIS data. Remote Sensing, 10: 890.

Howell T.A., Schneider A.D., Dusek D.A., Marek T.H., Steiner J.L. (1995): Calibration and scale performance of Bushland weighing lysimeters. Transactions of the ASAE, 38: 1019–1024.

Huete A.R. (1988): A soil-adjusted vegetation index (SAVI). Remote Sensing of Environment, 25: 295–309.

Huete A., Didan K., Miura T., Rodriguez E., Gao X., Ferreira L. (2002): Overview of the radiometric and biophysical performance of the MODIS vegetation indices. Remote Sensing of Environment, 83: 195–213.

Irmak S., Skaggs K.E., Chatterjee S. (2014): A review of the Bowen ratio surface energy balance method for quantifying evapotranspiration and other energy fluxes. Transactions of the ASABE, 57: 1657–1674.

Jensen M.E., Wright J.L. (1978): The role of evapotranspiration models in irrigation scheduling. Transactions of the ASAE, 21: 82–87.

Jeřábek J., Zumr D., Dostál T. (2017): Identifying the plough pan position on cultivated soils by measurements of electrical resistivity and penetration resistance. Soil and Tillage Research, 174: 231–240.

Jeřábek J., Zumr D., Laburda T., Krása J., Dostál T. (2022): Soil surface connectivity of tilled soil with wheel tracks and its development under simulated rainfall. Journal of Hydrology, 613: 128322.

Kendall M.G., Stuart A. (1969): The Advanced Theory of Statistics. 3rd Ed. Griffin, London, High Wycombe.

Kimm H., Guan K., Jiang C., Peng B., Gentry L.F., Wilkin S.C., Wang S., Cai Y., Bernacchi C. J., Peng J., Luo Y. (2020): Deriving high-spatiotemporal-resolution leaf area index for agroecosystems in the U.S. Corn Belt using Planet Labs CubeSat and STAIR fusion data. Remote Sensing of Environment, 239: 111615.

Kokhan S., Vostokov A. (2020): Using Vegetative indices to quantify agricultural crop characteristics. Journal of Ecological Engineering, 21: 120–127.

Li T., Jeřábek J., Noreika N., Dostál T., Zumr D. (2021): An overview of hydrometeorological datasets from a small agricultural catchment (Nučice) in the Czech Republic. Hydrological Processes, 35: e14042.

Li W., Migliavacca M., Forkel M., Denissen J.M.C., Reichstein M., Yang H., Duveiller G., Weber U., Orth R. (2022): Widespread increasing vegetation sensitivity to soil moisture. Nature Communications, 13: 3959.

Marek T., Piccinni G., Schneider A., Howell T., Jett M., Dusek D. (2006): Weighing lysimeters for the determination of crop water requirements and crop coefficients. Applied Engineering in Agriculture, 22: 851–856.

Martin K.L., Girma K., Freeman K.W., Teal R.K., Tubańa B., Arnall D.B., Chung B., Walsk O., Solie J.B., Stone M.L., Raun W.R. (2007): Expression of variability in corn as influenced by growth stage using optical sensor measurements. Agronomy Journal, 99: 384–389.

Martínez B., Gilabert M.A. (2009): Vegetation dynamics from NDVI time series analysis using the wavelet transform. Remote Sensing of Environment, 113: 1823–1842.

McCabe M.F., Rodell M., Alsdorf D.E., Miralles D.G., Uijlenhoet R., Wagner W., Lucieer A., Houborg R., Verhoest N.E.C., Franz T.E., Shi J., Gao H., Wood E.F. (2017): The future of earth observation in hydrology. Hydrology and Earth System Sciences, 21: 3879–3914.

Meijninger W.M.L., Hartogensis O.K., Kohsiek W., Hoedjes J.C.B., Zuubier R.M., De Bruin H.A.R. (2002): Determination of area-averaged sensible heat fluxes with a large aperture scintillometer over a heterogeneous surface – Flevoland field experiment. Boundary-Layer Meteorology, 105: 37–62.

Nagler P.L., Cleverly J., Glenn E., Lampkin D., Huete A., Wan Z. (2005): Predicting riparian evapotranspiration from MODIS vegetation indices and meteorological data. Remote Sensing of Environment, 94: 17–30.

Nagler P., Glenn E., Nguyen U., Scott R., Doody T. (2013): Estimating riparian and agricultural actual evapotranspiration by reference evapotranspiration and MODIS enhanced vegetation index. Remote Sensing, 5: 3849–3871.

Nagler P.L., Barreto-Muñoz A., Chavoshi Borujeni S., Jarchow C.J., Gómez-Sapiens M.M., Nouri H., Herrmann S.M., Didan K. (2020): Ecohydrological responses to surface flow across borders: Two decades of changes in vegetation greenness and water use in the riparian corridor of the Colorado River delta. Hydrological Processes, 34: 4851–4883.

https://doi.org/10.17221/60/2023-SWR

Nash J.E., Sutcliffe J.V. (1970): River flow forecasting through conceptual models part I — A discussion of principles. Journal of Hydrology, 10: 282–290.

Nguyen T.T., Ngo H.H., Guo W., Chang S.W., Nguyen D.D., Nguyen C.T., Zhang J., Liang S., Bui X.T., Hoang N.B. (2022): A low-cost approach for soil moisture prediction using multi-sensor data and machine learning algorithm. Science of the Total Environment, 833: 155066.

Nguy-Robertson A.L., Peng Y., Gitelson A.A., Arkebauer T.J., Pimstein A., Herrmann I., Karnieli A., Rundquist D.C., Bonfil D.J. (2014): Estimating green LAI in four crops: Potential of determining optimal spectral bands for a universal algorithm. Agricultural and Forest Meteorology, 192–193: 140–148.

Noreika N., Li T., Zumr D., Krasa J., Dostal T., Srinivasan R. (2020): Farm-scale biofuel crop adoption and its effects on in-basin water balance. Sustainability (Switzerland), 12: 10596.

Noreika N., Winterová J., Li T., Krása J., Dostál T. (2021): The small water cycle in the Czech landscape: How has it been affected by land management changes over time? Sustainability (Switzerland), 13: 13757.

Noreika N., Li T., Winterova J., Krasa J., Dostal T. (2022): The effects of agricultural conservation practices on the small water cycle: From the farm-to the management-scale. Land, 11: 683.

Park J., Baik J., Choi M. (2017): Satellite-based crop coefficient and evapotranspiration using surface soil moisture and vegetation indices in Northeast Asia. Catena, 156: 305–314.

Priestley C.H.B., Taylor R.J. (1972): On the assessment of surface heat flux and evaporation using large-scale parameters. Monthly Weather Review, 100: 81–92.

Robinson D.A., Jones S.B., Wraith J.M., Or D., Friedman S.P. (2003): A review of advances in dielectric and electrical conductivity measurement in soils using time domain reflectometry. Vadose Zone Journal, 2: 444–475.

Rong L., Duan X., Feng D., Zhang G. (2017): Soil moisture variation in a farmed dry-hot valley catchment evaluated by a redundancy analysis approach. Water, 9: 92.

Rouse J.W., Haas R.H., Schell J.A., Deering D.W. (1973): Monitoring vegetation systems in the great plains with ERTS. NASA Special Publication, 351: 309.

Schiavo M. (2022): Probabilistic delineation of subsurface connected pathways in alluvial aquifers under geological uncertainty. Journal of Hydrology, 615: 128674.

Schiavo M., Riva M., Guadagnini L., Zehe E., Guadagnini A. (2022): Probabilistic identification of Preferential Groundwater Networks. Journal of Hydrology, 610: 127906.

Shafian S., Rajan N., Schnell R., Bagavathiannan M., Valasek J., Shi Y., Olsenholler J. (2018): Unmanned aerial systems-based remote sensing for monitoring sorghum growth and development. PLoS ONE, 13: e0196605.

Sharma R., Bhandari R. (2015): Skewness, kurtosis and Newton's inequality. Rocky Mountain Journal of Mathematics, 45: 1639–1643.

Stocker B.D., Tumber-Dávila S.J., Konings A.G., Anderson M.C., Hain C., Jackson R.B. (2023): Global patterns of water storage in the rooting zones of vegetation. Nature Geoscience, 16: 250–256.

Tenreiro T.R., Jeřábek J., Gómez J.A., Zumr D., Martínez G., García-Vila M., Fereres E. (2022): Simulating water lateral inflow and its contribution to spatial variations of rainfed wheat yields. European Journal of Agronomy, 137: 126515.

Topp G.C., Davis J.L., Annan A.P. (1980): Electromagnetic determination of soil water content: Measurements in coaxial transmission lines. Water Resources Research, 16: 574–582.

Trautmann T., Koirala S., Carvalhais N., Güntner A., Jung M. (2022): The importance of vegetation in understanding terrestrial water storage variations. Hydrology and Earth System Sciences, 26: 1089–1109.

Tucker C.J. (1979): Red and photographic infrared linear combinations for monitoring vegetation. Remote Sensing of Environment, 8: 127–150.

Ukasha M., Ramirez J.A., Niemann J.D. (2022): Temporal variations of NDVI and LAI and interactions with hydroclimatic variables in a large and agro-ecologically diverse region. Journal of Geophysical Research: Biogeosciences, 127: e2021JG006395.

Wang K., Li Z., Cribb M. (2006): Estimation of evaporative fraction from a combination of day and night land surface temperatures and NDVI: A new method to determine the Priestley–Taylor parameter. Remote Sensing of Environment, 102: 293–305.

Wang K., Wang P., Li Z., Cribb M., Sparrow M. (2007): A simple method to estimate actual evapotranspiration from a combination of net radiation, vegetation index, and temperature. Journal of Geophysical Research, 112: D15107.

Wilson K., Goldstein A., Falge E., Aubinet M., Baldocchi D., Berbigier P., Bernhofer C., Ceulemans R., Dolman H., Field C., Grelle A., Ibrom A., Law B., Kowalski A., Meyers T., Moncrieff J., Monson R., Oechel W., Tenhunen J., Valentini R., Verma S. (2002): Energy balance closure at FLUXNET sites. Agricultural and Forest Meteorology, 113: 223–243.

Wohlfahrt G., Tasser E. (2015): A mobile system for quantifying the spatial variability of the surface energy balance: Design and application. International Journal of Biometeorology, 59: 617–627.

https://doi.org/10.17221/60/2023-SWR

Wyatt B.M., Ochsner T.E., Zou C.B. (2021): Estimating root zone soil moisture across diverse land cover types by integrating in-situ and remotely sensed data. Agricultural and Forest Meteorology, 307: 108471.

Yuan W., Liu S., Yu G., Bonnefond J.-M., Chen J., Davis K., Desai A.R., Goldstein A.H., Gianelle D., Rossi F., Suyker A.E., Verma S.B. (2010): Global estimates of evapotranspiration and gross primary production based on MODIS and global meteorology data. Remote Sensing of Environment, 114: 1416–1431.

Zhang Y., Wegehenkel M. (2006): Integration of MODIS data into a simple model for the spatial distributed simulation of soil water content and evapotranspiration. Remote Sensing of Environment, 104: 393–408.

Zhang Y., Wang K., Wang J., Liu C., Shangguan Z. (2021): Changes in soil water holding capacity and water availability following vegetation restoration on the Chinese Loess Plateau. Scientific Reports, 11: 9692.

Ziliani M.G., Altaf M.U., Aragon B., Houburg R., Franz T.E., Lu Y., Sheffield J., Hoteit I., McCabe M.F. (2022): Early season prediction of within-field crop yield variability by assimilating CubeSat data into a crop model. Agricultural and Forest Meteorology, 313: 108736.

Zumr D., Dostál T., Devátý J. (2015): Identification of prevailing storm runoff generation mechanisms in an intensively cultivated catchment. Journal of Hydrology and Hydromechanics, 63: 246–254.

Received: June 21, 2023
Accepted: September 5, 2023
Published online: October 3, 2023